Histopathologic Validation of 3′-Deoxy-3′-^{18}F-Fluorothymidine PET in Squamous Cell Carcinoma of the Oral Cavity

Esther G.C. Troost[1], Johan Bussink[1], Piet J. Slootweg[2], Wenny J.M. Peeters[1], Matthias A.W. Merkx[3], Albert J. van der Kogel[1], Wim J.G. Oyen[4], and Johannes H.A.M. Kaanders[1]

[1]Department of Radiation Oncology, Institute of Oncology, Radboud University Nijmegen Medical Centre, Nijmegen, The Netherlands; [2]Department of Pathology, Institute of Oncology, Radboud University Nijmegen Medical Centre, Nijmegen, The Netherlands; [3]Department of Maxillofacial Surgery, Institute of Oncology, Radboud University Nijmegen Medical Centre, Nijmegen, The Netherlands; and [4]Department of Nuclear Medicine, Institute of Oncology, Radboud University Nijmegen Medical Centre, Nijmegen, The Netherlands

Accelerated tumor cell repopulation is an important mechanism adversely affecting therapeutic outcome in head and neck cancer. The noninvasive assessment of the proliferative state of a tumor by PET may provide a selection tool for customized treatment. 3′-deoxy-3′-^{18}F-fluorothymidine (^{18}F-FLT) is a PET tracer that is phosphorylated by thymidine kinase 1 (TK-1) and, as such, reflects cellular proliferation. Before the use of ^{18}F-FLT PET for tumor characterization is accepted and introduced into clinical studies, validation against tumor histology is mandatory. The aim of this study was to validate ^{18}F-FLT PET in squamous cell carcinomas of the oral cavity using immunohistochemical staining for the proliferation marker iododeoxyuridine and for TK-1. **Methods:** Seventeen patients with primary squamous cell carcinomas of the oral cavity underwent an ^{18}F-FLT PET/CT scan before surgery, and iododeoxyuridine was administered 20 min before tumor resection. ^{18}F-FLT PET/CT scans were segmented, and PET/CT volumes and PET signal intensities were calculated (mean standardized uptake value [SUV_{mean}] and maximum standardized uptake value [SUV_{max}]). Multiple paraffin-embedded tumor sections were immunohistochemically stained for iododeoxyuridine and TK-1. For iododeoxyuridine, labeling indices and optical densities were calculated and correlated with SUV_{mean} and SUV_{max}. TK-1 staining was visually and semiquantitatively assessed. **Results:** All primary tumors were identified with ^{18}F-FLT PET but with a large range in tracer uptake (mean SUV_{max}, 5.9; range, 2.2–15.2). Also, there was a large variability in iododeoxyuridine labeling indices (mean, 0.09; range, 0.01–0.29) and optical densities (mean, 28.2; range, 12.6–37.8). The iododeoxyuridine optical densities correlated significantly with SUV_{mean} and SUV_{max}, but the labeling indices did not. In most tumors, TK-1 staining of varying intensity was present but correlated with neither iododeoxyuridine binding nor ^{18}F-FLT uptake. **Conclusion:** The current study demonstrated only a weak correlation between ^{18}F-FLT uptake and iododeoxyuridine staining intensity in oral cavity tumors. This weak correlation may be explained by differences in biomarker characteristics, resolution, and quantification methods.

Key Words: ^{18}F-fluorothymidine PET; proliferation; head and neck cancer; immunohistochemistry; iododeoxyuridine; thymidine kinase

J Nucl Med 2010; 51:713–719
DOI: 10.2967/jnumed.109.071910

PET with the glucose analog ^{18}F-FDG is accepted as a powerful, noninvasive metabolic imaging method suitable for the diagnosis and staging of various types of cancer (*1*). Tumor cell repopulation is an important indicator of tumor aggressiveness and of its resistance to various types of treatment. As a response to radiation therapy, squamous cell carcinomas of the head and neck show accelerated repopulation of clonogenic tumor cells during the course of treatment that adversely affects treatment outcome (*2–5*). Randomized trials have convincingly shown that the reduction of the overall treatment time by accelerated radiotherapy schedules increases the locoregional tumor control rate by about 10% (*6–8*). Targeting the signal transduction pathways that control tumor cell proliferation by inhibition of the epidermal growth factor receptor in combination with radiotherapy improves not only local tumor control but also ultimate survival (*9,10*).

Noninvasive assays monitoring the proliferative activity of the tumor before and during therapy may assist in better patient selection for these intensified treatment strategies. The thymidine analog 3′-deoxy-3′-^{18}F-fluorothymidine (^{18}F-FLT) serves as a PET tracer for visualization of proliferating (tumor) cells (*11*). ^{18}F-FLT is transported via the membranous human nucleoside transporter 1, phosphorylated by the cytosolic thymidine kinase 1 (TK-1) enzyme, and trapped intracellularly (*12*). During the late G_1 and S phases of the cellular cycle, TK-1 enzyme activity

Received Oct. 26, 2009; revision accepted Feb. 2, 2010.
For correspondence or reprints contact: Esther G.C. Troost, Department of Radiation Oncology, Institute of Oncology, Radboud University Nijmegen Medical Centre, P.O. Box 9101, 6500 HB Nijmegen, The Netherlands.
E-mail: e.troost@rther.umcn.nl

increases by almost 10-fold. As ^{18}F-FLT trapping is related to TK-1 activity, it is in turn also linked to cellular proliferation (*13,14*).

Before treatment decisions can be based on these functional imaging modalities, it is of utmost importance to perform histologic validation studies. Quantitative ^{18}F-FLT PET data must be correlated with quantitative data of proliferation at the tissue and cellular levels obtained by histologic examination.

The first aim of this study was to validate ^{18}F-FLT PET by immunohistochemical staining of the exogenous proliferation marker iododeoxyuridine and TK-1, the enzyme phosphorylating ^{18}F-FLT, in primary resection specimens of oral cavity tumors. Second, the resection specimens were stained for the endogenous proliferation marker Ki-67 for ^{18}F-FLT PET validation purposes.

MATERIALS AND METHODS

Patients

From July 2005 to March 2008, 17 patients with newly diagnosed clinical stage II–IV primary squamous cell carcinoma of the oral cavity eligible for surgical tumor resection were included in this study after giving written informed consent. The Institutional Review Board of the Radboud University Nijmegen Medical Centre approved this study.

^{18}F-FLT Synthesis

^{18}F-FLT was obtained from the Department of Nuclear Medicine and PET Research, VU University Medical Centre, Amsterdam, The Netherlands. Synthesis was performed as described previously (*15,16*).

PET/CT Acquisition

Before the surgical tumor resection, integrated PET and CT images were acquired on either a hybrid PET/CT scanner or by means of software fusion of dedicated stand-alone PET and CT images. All scans were obtained with the patients supine and fixed in a rigid customized mask covering the head and neck area, to increase position accuracy and to reduce movement artifacts during PET/CT.

Hybrid PET/CT images were acquired using a Biograph Duo scanner (Siemens/CTI). Emission images of the head and neck area were recorded 60 min after intravenous injection of approximately 250 MBq of ^{18}F-FLT, with 7 min per bed position in 3-dimensional mode. PET images were reconstructed using the ordered-subset expectation maximization iterative algorithm with parameters optimized for the head and neck area (i.e., 4 iterations, 16 subsets, and 5-mm 3-dimensional gaussian filter (*17*)), with correction for photon attenuation. In addition, CT images were acquired for anatomic correlation and attenuation correction using 80 mAs, 130 kV, a 3-mm slice width, and a venous phase intravenous contrast agent (Optiray; Mallinckrodt Inc.).

Dedicated PET images were acquired using an ECAT Exact scanner (Siemens/CTI). Emission and transmission images of the head and neck area were recorded 60 min after intravenous injection of approximately 250 MBq of ^{18}F-FLT, with 5 min per bed position in 3-dimensional mode for emission and 3 min per bed position in 2-dimensional mode for transmission. PET image reconstruction parameters were identical to the hybrid PET/CT parameters. Dedicated CT images were acquired using an AcQsim CT scanner (Philips), applying the same acquisition parameters as those for the hybrid PET/CT. PET and CT image sets were anatomically coregistered using iterative closest point–based optimization of surface maps derived from PET transmission and CT images, with an average registration accuracy of 3 mm (*18*).

PET Tracer Uptake Analysis and Image Segmentation

After reconstruction and coregistration, standardized uptake value (SUV) PET images were created with software developed in-house, which corrected for injected dose, tracer decay, and patient body weight. Subsequently, these SUV PET images were resliced using the CT image as reference. SUV PET and CT images were imported into Pinnacle^3 (version 8.0d; Philips Radiation Oncology System), the radiotherapy planning system routinely used at our department.

The gross tumor volume (GTV) was first delineated on CT. Self-written scripts in Pinnacle^3 aided with the segmentation of the primary tumor and with the calculation of the mean and maximum standardized uptake value (SUV_{mean} and SUV_{max}, respectively) from the PET data. For segmentation of the PET images, an adaptive threshold delineation based on the signal-to-background ratio (GTV_{SBR}) was performed (*19*). For this mean, the SUV_{max} was defined as mean activity of the hottest voxel in the tumor and its 8 surrounding voxels in a transversal slice. Mean background activity was acquired in a manually defined region of interest in the left neck musculature (~10 cm^3) at a sufficient distance from the primary tumor, metastatic cervical lymph nodes, and vertebrae. Within the segmented volumes, the SUV_{mean} and SUV_{max} were calculated.

Administration of Iododeoxyuridine and Immunohistochemical Staining for Iododeoxyuridine, Ki-67, and TK-1

Twenty minutes before the start of surgery, iododeoxyuridine (Centre Hospitalier Universitaire Vaudois) (200 mg diluted in 100 mL of NaCl 0.9%) was administered intravenously as a bolus injection.

The paraffin blocks containing the resection material from the 17 primary oral cavity tumors were collected from the Pathology Department. To obtain a representative sample of the tumor, we aimed at collecting 3 blocks per patient, 1 from the tumor center and 2 localized more peripherally.

From these blocks, 5-μm consecutive sections were stained for iododeoxyuridine, Ki-67, and TK-1. The staining protocols for iododeoxyuridine and Ki-67 have been described elsewhere (*16*). For TK-1 staining, primary tumor sections were rinsed with 0.1 M phosphate-buffered saline (Klinipath), pH 7.4, between all steps of this procedure. The staining procedure was performed at room temperature unless stated differently. The sections were deparaffinized and rehydrated in Histosafe (Adamas Instrumenten B.V.) and graded alcohols (100%−96%−70%). For antigen retrieval, slides were heated (90°C) in 10 mM citrate buffer, pH 6.0, for 30 min (DAKO). The endogenous peroxidase was blocked with 3% H_2O_2 in methanol for 10 min, followed by preincubation with primary antibody diluent (GeneTex Inc.) and incubation with 5% normal donkey serum diluted in primary antibody diluent for 30 min. Finally, sections were incubated overnight with mouse anti-TK-1 (AbD Serotec), diluted 1:800 in primary antibody diluent at 4°C. Next, all sections were incubated with donkey–antimouse–biotin

(Jackson Immuno Research Laboratories), diluted 1:200 (TK-1) in phosphate-buffered saline for 60 min, and subsequently diluted with avidin-biotin complex reagent (Vector Laboratories) for 30 min. Then, sections were rinsed with deionized water before incubation with diaminobenzidine (Zymed Laboratories) for 15 min. Finally, after rinsing with tap water and staining with hematoxylin (Klinipath) for 30 s, sections were dehydrated and captured in mounting medium (Klinipath).

Immunohistochemical Image Acquisition and Image Processing

Iododeoxyuridine and Ki-67 Labeling Index and Optical Density. After immunohistochemical staining, the entire tumor sections were scanned at ×200 magnification using a digital image-processing system consisting of a color charge-coupled device camera (Retiga SRV, 1,392 × 1,040 pixels; QImaging) and a red, green, blue filter (Slider Module; QImaging) attached to a motorized bright field microscope (DM6000; Leica). Whole-tumor sections were scanned using a Macintosh computer (Apple Inc.) running IPLab (Scanalytics Inc.), which controlled this motorized system and generated 24-bit color composite images. For every scan session, separate background images were recorded. To extract and separate the color information from the diaminobenzidine and hematoxylin signals, the red, green, blue linear unmixing module in the TRI2 software (Apple Inc.) was applied using the absorption mode (*20*). For this procedure, reference files from single-stained control sections were used containing color information for the blue (hematoxylin; all nuclei) and brown (proliferating nuclei) signal. Additionally, each red, green, blue color image was corrected for the microscope illumination using the background image and was subsequently normalized. Next, threshold values for the diaminobenzidine and hematoxylin signal were manually set. For the image analysis, a tumor mask was delineated including tumor, intratumoral stroma, and areas of necrosis but excluding surrounding normal tissues. Within this mask, the labeling index for iododeoxyuridine and Ki-67 was calculated by dividing the diaminobenzidine-positive area (representing nuclei positive for iododeoxyuridine or Ki-67) by the hematoxylin area (representing all nuclei).

To adjust for different sizes of immunohistochemically stained nuclei and for variation in the staining intensity for iododeoxyuridine and Ki-67, mean optical densities were calculated for the entire tumor area using a Macintosh computer running IPLab.

Analysis of Immunohistochemical Staining for TK-1. Because of a relatively weak immunohistochemical staining of TK-1 in most of the tumors, automated quantitative analyses were not possible. Therefore, 2 investigators, who were unaware of the results obtained by PET and iododeoxyuridine immunohistochemistry, visually and semiquantitatively assessed the entire tumor sections, using ×200 magnification. The percentage of positive cells, their localization, and the staining intensity were estimated. Staining intensity was classified as no staining, weak staining visible only under high magnification, and strong staining also visible under lower magnification. The combination of staining intensity with percentage of positive cells resulted in 4 categories: absence of TK-1 staining, weak and sparse (≤5%) staining, weak and abundant (>5%−20%) staining, and strong and abundant (>5%−20%) staining. There were no tumors with strong and sparse TK-1 staining. Agreement on all tumor sections was achieved before further analysis. TK-1 staining categories were subsequently correlated to the SUV_{max} of ^{18}F-FLT PET, iododeoxyuridine labeling indices, and iododeoxyuridine optical densities.

Statistical Analysis

Statistical analyses were performed using GraphPad Prism (version 4.0c; GraphPad Software) for Macintosh. Gaussian distribution of the values was analyzed using the Kolmogorov–Smirnov test. GTV first delineated on CT and GTV_{SBR} were compared using a 2-tailed Mann–Whitney test. SUVs for PET with iododeoxyuridine and Ki-67 labeling indices were correlated using the 2-tailed Pearson test. Linear regression was performed for the SUV and iododeoxyuridine and Ki-67 optical densities under the assumption that an optical density of zero resulted in an SUV of zero for ^{18}F-FLT PET. The results of the semiquantitative analysis for TK-1 versus the SUV_{max}, iododeoxyuridine and Ki-67 labeling indices, and optical densities were analyzed using a Kruskal–Wallis test. A P value less than or equal to 0.05 was regarded as statistically significant.

RESULTS

Patient and Tumor Characteristics

Thirteen men and 4 women, with an average age of 57 y, participated in this study. Patient and tumor characteristics are given in Table 1. Most tumors were clinically and pathologically classified as T2. Patients 1–3 were scanned on the dedicated CT and PET machines on the same day; the other patients underwent ^{18}F-FLT PET/CT on the hybrid scanner. The median interval between PET/CT scan and surgery was 5 d (range, 2–36 d). The longest interval of 36 d was caused by an intercurrent infection, which delayed the surgery.

^{18}F-FLT Uptake in Primary Tumor

^{18}F-FLT PET data were available for all 17 patients, and all primary tumors were detected by ^{18}F-FLT PET, as opposed to only 12 by contrast-enhanced CT (Supplemental Fig. 1; supplemental materials are available online only at http://jnm.snmjournals.org). The mean GTV first delineated on CT ± SD (13.6 ± 8.2 cm^3) was significantly larger than the mean GTV_{SBR} (7.2 ± 5.6 cm^3; $P = 0.03$). The mean ^{18}F-FLT SUV_{max} in the primary tumors was 5.9 ± 3.2, and the mean SUV_{mean} within the GTV_{SBR} was 4.0 ± 2.2.

Iododeoxyuridine Labeling Index and Optical Density and Correlations with ^{18}F-FLT PET

No adverse events occurred during the intravenous administration of iododeoxyuridine or ^{18}F-FLT. Paraffin blocks containing primary tumor tissue were available from all 17 patients. We aimed at collecting 3 blocks per patient, 1 from the tumor center and 2 more peripherally. However, only 1 block was available for 6 patients, 2 blocks were retrieved for 7 patients, and 3 tumor blocks were available for the remaining 4 patients, because the tumor tissue was present in only 1 or 2 blocks in most cases. In all tumor sections, tumor cells stained positively for iododeoxyuridine, and in 2 cases, iododeoxyuridine staining was also present in peritumoral inflammatory tissue (Fig. 1A). There

TABLE 1. Patient Characteristics, Clinical and Pathologic Stages, and Therapeutic Procedures

Patient no.	Site	Sex	Age (y)	Surgical procedure	Clinical stage	Pathologic stage	Tumor grade
1	Lower alveolar ridge	M	46	TE + MRND, right	T4N2bM0	pT4pN0M0	2
2	Floor of mouth	F	53	TE + bilateral SND	T2N0M0	pT2pN0M0	2
3	Tongue	M	43	TE + SND, right	T3N0M0	pT3pN1M0	3
4	Tongue	M	70	TE + MRND, left	T4N0M0	pT2pN0M0	2
5	Floor of mouth	M	61	TE + SND, left	T2N0M0	pT2pN0M0	2
6	Floor of mouth	F	49	TE + SND, right	T2N0M0	pT2pN0M0	2
7	Floor of mouth	M	72	TE + MRND, right	T4N2bM0	pT2pN2bM0	3
8	Retromolar trigone	M	75	TE + SND, left	T4N0M0	pT4pN1M0	3
9	Hard palate	M	54	TE	T4N0M0	pT4pN0M0	2
10	Tongue/floor of mouth	M	62	TE + SND, left, + MRND, right	T2N1M0	pT2pN2bM0	3
11	Tongue	F	45	TE + bilateral MRND	T4N2cM0	pT4pN2cM0	3
12	Floor of mouth	M	53	TE + MRND, right	T2N1M0	pT2pN1M0	2
13	Floor of mouth	M	56	TE + MRND, left	T3N0M0	pT1pN2bM0	2
14	Tongue	M	67	TE + SND, right	T2N0M0	pT1pN0M0	2
15	Tongue/floor of mouth	M	45	TE + MRND, left	T2N1M0	pT2pN2bM0	2
16	Tongue	F	59	TE + bilateral SND	T2N0M0	pT2pN2bM0	2
17	Tongue	M	43	TE + SND, left	T2N0M0	pT1pN1M0	2

TE = tumor excision; MRND = modified radical neck dissection; SND = supraomohyoid neck dissection (levels I–III).

was a large variability in iododeoxyuridine labeling indices, with a mean value of 0.09 and an SD of ±0.14 (range, 0.01–0.29). Furthermore, there was a large range in optical densities for iododeoxyuridine, with a mean of 28.2 ± 12.7 (range, 12.6–37.8). There was no statistically significant correlation between the mean iododeoxyuridine labeling index and the SUV_{max} or SUV_{mean} of ^{18}F-FLT PET (Fig. 2A; data for SUV_{mean} not shown). In contrast to this, the signal intensities (i.e., optical densities for immunohistochemical iododeoxyuridine staining vs. ^{18}F-FLT PET SUV_{max} and SUV_{mean}) demonstrated a significant, albeit weak, correlation ($P < 0.0001$; Fig. 2B; data for SUV_{mean} not shown).

Ki-67 Labeling Index and Optical Density and Correlations with ^{18}F-FLT PET

As for iododeoxyuridine, there was no statistically significant correlation between the mean Ki-67 labeling index and the SUV_{max} or SUV_{mean} of ^{18}F-FLT PET (Supplemental Fig. 2A; data for SUV_{mean} not shown). However, the optical densities for Ki-67 staining versus ^{18}F-FLT PET SUV_{max} and SUV_{mean} demonstrated a significant, albeit weak, correlation ($P < 0.0001$; Supplemental Fig. 2B; data for SUV_{mean} not shown).

TK-1 Staining and Correlations with Iododeoxyuridine and ^{18}F-FLT PET

In 13 oral cavity tumors, TK-1 staining was found in the cytoplasm of tumor cells, with an intensity ranging from weak to intense (Figs. 1A−1C). In 1 tumor, TK-1 staining was predominantly localized in the invasive tumor front (Fig. 1D). Overall, staining for TK-1 was substantially weaker than for iododeoxyuridine, and fewer tumor cells stained positively. Mostly, TK-1 and iododeoxyuridine colocalized in the same tumor areas, but correlation at the cellular level could not be assessed, because the stainings were performed on consecutive sections.

After semiquantitative analysis of TK-1 staining, 4 categories were identified on the basis of staining intensity and percentage of positive cells. These categories were correlated to the SUV_{max} of ^{18}F-FLT PET (Fig. 3A), iododeoxyuridine labeling indices (Fig. 3B), and iododeoxyuridine optical densities (Fig. 3C). However, no statistically significant correlations between these parameters were found.

DISCUSSION

In primary squamous cell carcinomas of the oral cavity, we validated ^{18}F-FLT PET against immunohistochemical staining of the exogenous proliferation marker iododeoxyuridine, immunohistochemical staining of the endogenous marker Ki-67, and immunohistochemical expression of the TK-1 enzyme.

In oral cavity tumors, we found a relatively high mean SUV_{max} for ^{18}F-FLT PET. The sensitivity for tumor detection was high (100%) in comparison to contrast-enhanced CT (76%), which was hampered by the relatively small tumor size and dental artifacts. Lower SUV_{max} (mean, 1.6; range, 1.0–5.7) was observed in laryngeal tumors with a lower sensitivity (88%), possibly because of the generally smaller volumes of laryngeal carcinomas (*21*). Two other publications involving head and neck cancers of various sites and non–small cell lung cancer both reported a mean SUV_{max} of 4.8 (*22,23*).

The GTVs delineated after segmentation of the PET signal (GTV_{SBR}) were significantly smaller than the GTVs manually delineated on contrast-enhanced CT scans. A similar finding has previously been reported for laryngeal tumors using ^{18}F-FDG PET (*24*). Daisne et al. (*24*) found

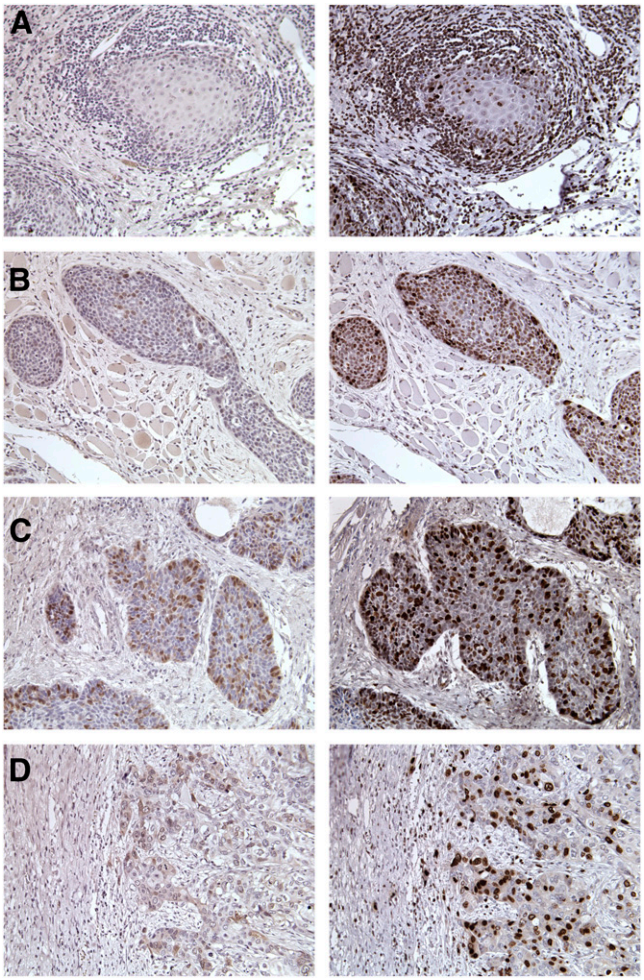

FIGURE 1. Immunohistochemical staining for TK-1 (left; brown), iododeoxyuridine (right; brown), and nuclei (blue) in adjacent sections of squamous cell carcinomas of oral cavity. Absence of staining for TK-1 and intense staining for iododeoxyuridine in tumor and adjacent inflammatory cells (A), weak staining for TK-1 and intense staining for iododeoxyuridine in tumor cells (B), intense staining for TK-1 and iododeoxyuridine in tumor cells (C), and positive staining for both markers (TK-1, weak; iododeoxyuridine, strong) in invasive front of squamous cell carcinoma (D).

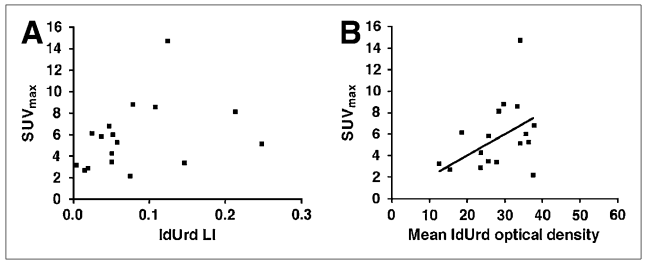

FIGURE 2. (A) Two-tailed Pearson correlation of mean iododeoxyuridine labeling indices with SUV_{max} for all squamous cell carcinomas of oral cavity; $P = 0.18$, $r^2 = 0.12$. (B) Linear regression analysis of mean iododeoxyuridine optical densities vs. SUV_{max}; $P < 0.0001$. IdUrd = iododeoxyuridine; LI = labeling indices.

the GTVs using PET, compared with CT and MRI, to be the smallest. Furthermore, these GTVs, compared with laryngeal resection specimens, were the most accurate.

However, the potential application of ^{18}F-FLT PET in oncology may not be so much in improving the sensitivity of tumor detection or its anatomic extensions as in characterizing the biologic behavior of a tumor. Therefore, we compared quantitative analysis of ^{18}F-FLT uptake with standard methods for quantification of proliferation by immunohistochemical markers. Iododeoxyuridine is an S phase–specific marker of proliferation. It was hypothesized that iododeoxyuridine binding should correlate with ^{18}F-FLT uptake, because the activity of TK-1—the key enzyme in ^{18}F-FLT phosphorylation—is also mainly upregulated during the S phase (*25*). Somewhat unexpectedly, we did not find a correlation between the iododeoxyuridine labeling indices and the ^{18}F-FLT SUV_{max} or SUV_{mean}. This may be due to the relatively unstable nature of iododeoxyuridine because of deiodination. Therefore, we also correlated the SUV_{max} and SUV_{mean} with Ki-67 but did not find a significant positive correlation either. In contrast to our findings, several studies on different tumor types found significant positive correlations between SUVs for ^{18}F-FLT PET and proliferation assessed by Ki-67 immunohistochemistry, whereas 3 other studies in thoracic, breast, and gastric tumors did not demonstrate such a correlation (*26–29*). This discrepancy may also be caused by the different underlying histopathology (non–small cell lung cancer, adenocarcinoma of the breast, and lymphoma as opposed to squamous cell carcinomas of the oral cavity).

There are several factors that potentially play a role in the lack of correlation between iododeoxyuridine labeling indices and ^{18}F-FLT PET SUVs in the current study. (1) The principal enzyme for ^{18}F-FLT uptake, TK-1, is involved in the salvage pathway of DNA synthesis. When DNA synthesis is blocked, TK-1 can be upregulated through feedback mechanisms and result in increased ^{18}F-FLT uptake, whereas iododeoxyuridine uptake and thus staining remain unchanged. (2) For most patients, only 1 or 2 paraffin-embedded blocks containing tumor tissue were available, and from each block a single section was analyzed. Thus, only a relatively small tumor volume was assessed, with the inherent risk of sampling error, compared with the entire tumor volume characterized by ^{18}F-FLT PET. However, in contrast to studies by others, we tried to minimize this error by analyzing at least 2 tumor-containing paraffin blocks in 11 of the 17 patients and by examining the entire tumor sections. (3) There was an interval of several days between PET and surgery. However, compared with other studies reported in the literature, the median interval of 5 d was relatively short. Exclusion of the patients with an interval of more than 10 d did not alter the results and conclusions of this study (data not shown). (4) The resolution of the imaging modalities profoundly

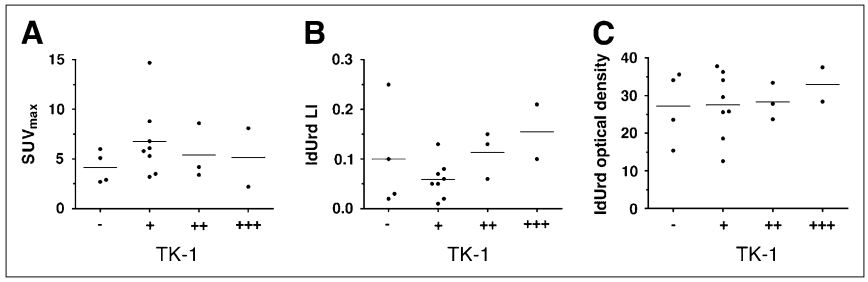

FIGURE 3. Kruskal–Wallis test of semiquantitative analysis of TK-1 staining (horizontal axis) correlating with SUV_{max} ($P = 0.44$) (A), iododeoxyuridine labeling indices ($P = 0.19$) (B), and iododeoxyuridine optical densities ($P = 0.75$) (C). TK-1 staining was categorized as absent (−), weak and sparse (+), weak and abundant (++), or strong and abundant (+++). IdUrd = iododeoxyuridine; LI = labeling indices.

differed (i.e., 2.5 μm for automatic analysis of bright-field microscopy of immunohistochemical sections as opposed to 5–8 mm using PET). (5) Different quantification procedures may influence the results. Some investigators assessed the mean labeling index or SUV_{mean}, whereas others calculated the respective SUV_{max}. Furthermore, these values were mostly estimated in the areas of highest proliferative activity or greatest staining intensity as opposed to complete tumor sections in our study. To specifically address this question, we also correlated the iododeoxyuridine labeling indices in the areas of highest proliferative activity with ^{18}F-FLT SUV, but again, this did not result in significant correlations (data not shown). The iododeoxyuridine labeling index is a measure of the relative number of tumor cells in S phase, as opposed to the ^{18}F-FLT SUV, which reflects the signal intensity of the tracer at a certain time point. ^{18}F-FLT uptake is determined by the tumor cells' DNA synthesis rate and might be better represented by the iododeoxyuridine staining intensity and less by labeling index. To test this, we assessed the iododeoxyuridine optical densities as a measure of staining intensity within the previously defined tumor areas. This approach yielded statistically significant, albeit weak, correlations with SUV_{max} and SUV_{mean} for ^{18}F-FLT (Fig. 2B). However, no significant results were found when comparing Ki-67 optical densities with ^{18}F-FLT SUVs (data not shown).

Finally, we assessed the expression of TK-1, the key enzyme involved in the exogenous (salvage) pathway of DNA synthesis (*25*). We studied the intensity of staining, its localization, and the global colocalization with iododeoxyuridine. Most of the tumors stained positively for TK-1, although most of the staining was rather faint and present in only a few tumor cells. In the consecutive tumor sections, the area of cytoplasmatic TK-1 staining colocalized with nuclear staining for iododeoxyuridine on a global level, but correlation on a cellular level could not be assessed. There was no correlation between TK-1 staining intensity and number of TK-1–positive cells on the one hand and the ^{18}F-FLT SUV_{max}, the iododeoxyuridine labeling indices, or the iododeoxyuridine optical densities on the other.

TK-1 staining has been used for flow cytometric analyses (*30*), but experience with immunohistochemical staining for TK-1 in tumor sections is limited. A few groups have performed immunohistochemistry on histologic tumor sections of breast cancer, non–small cell lung cancer, and colorectal cancer patients (*31–34*). The TK-1 labeling indices reported in these 4 studies were high (50%−80%), compared with our experience in squamous cell carcinomas of the oral cavity (*31–34*). To date, only 1 study on head and neck squamous cell carcinoma xenografts has been published (*35*). Molthoff et al. (*35*) assessed the value of ^{18}F-FLT PET for treatment response monitoring in xenografted squamous cell carcinomas after fractionated irradiation and immunohistochemically stained tumor sections for TK-1. The authors reported a significant decrease in ^{18}F-FLT tumor–to–normal tissue ratios, whereas TK-1 expression in control and irradiated tumors remained similar. However, details regarding TK-1 staining intensity, localization, and labeling index were not provided.

There is a discrepancy between TK-1 immunohistochemistry and its enzymatic activity. Expression levels of TK-1 are relatively stable during the entire cell cycle, with a peak in the enzyme activity in the late G_1 and S phases. Therefore, the correlation of the S phase marker iododeoxyuridine with the enzyme activity of TK-1 might have been better performed by (fluorocytometric) TK-1 assays of fresh resection specimens (*36,37*).

On the basis of the current results, the value of TK-1 staining as a measure of proliferative activity in oral cavity tumors seems limited. However, further research is needed (e.g., studies on colocalization with standard proliferation markers at the cellular level) until definite conclusions can be drawn about its significance as a biomarker for tumor cell proliferation.

CONCLUSION

Noninvasive ^{18}F-FLT PET assessing the proliferative status of tumors may be a valuable aid for patient selection and treatment response monitoring in head and neck cancer, but it needs to be validated before introduction in the clinic. This validation study demonstrated only a weak correlation between ^{18}F-FLT uptake and iododeoxyuridine staining intensity in squamous cell carcinomas of the oral cavity. Immunohistochemical staining of TK-1, the key enzyme in ^{18}F-FLT phosphorylation, correlated with neither ^{18}F-FLT uptake nor the standard immunohistochemical proliferation

markers. This may be due to differences in biomarker characteristics, discrepancies in resolution of the imaging modalities, and differences in quantification methods. The role of ^{18}F-FLT PET for the characterization of other tumor entities is more evident.

ACKNOWLEDGMENTS

We thank the technologists from the Departments of Radiation Oncology and Nuclear Medicine for their assistance and excellent patient care. Furthermore, we thank Paul F.J.W. Rijken and Saskia E. Rademakers for their assistance with the immunohistochemical analyses. Aswin L. Hoffmann is acknowledged for providing the Pinnacle^3 scripts for PET image segmentation. This work was supported by EC FP6 funding (Biocare contract LSHC-CT-2004-505785) and by Junior Investigator Grant 2006-38 of the Radboud University Nijmegen Medical Centre, The Netherlands.

REFERENCES

1. Fletcher JW, Djulbegovic B, Soares HP, et al. Recommendations on the use of ^{18}F-FDG PET in oncology. *J Nucl Med.* 2008;49:480–508.
2. Kim JJ, Tannock IF. Repopulation of cancer cells during therapy: an important cause of treatment failure. *Nat Rev Cancer.* 2005;5:516–525.
3. Maciejewski B, Withers HR, Taylor JM, Hliniak A. Dose fractionation and regeneration in radiotherapy for cancer of the oral cavity and oropharynx: tumor dose-response and repopulation. *Int J Radiat Oncol Biol Phys.* 1989;16:831–843.
4. Petersen C, Zips D, Krause M, et al. Repopulation of FaDu human squamous cell carcinoma during fractionated radiotherapy correlates with reoxygenation. *Int J Radiat Oncol Biol Phys.* 2001;51:483–493.
5. Withers HR, Taylor JM, Maciejewski B. The hazard of accelerated tumor clonogen repopulation during radiotherapy. *Acta Oncol.* 1988;27:131–146.
6. Bourhis J, Overgaard J, Audry H, et al. Hyperfractionated or accelerated radiotherapy in head and neck cancer: a meta-analysis. *Lancet.* 2006;368:843–854.
7. Fu KK, Pajak TF, Trotti A, et al. A Radiation Therapy Oncology Group (RTOG) phase III randomized study to compare hyperfractionation and two variants of accelerated fractionation to standard fractionation radiotherapy for head and neck squamous cell carcinomas: first report of RTOG 9003. *Int J Radiat Oncol Biol Phys.* 2000;48:7–16.
8. Overgaard J, Hansen HS, Specht L, et al. Five compared with six fractions per week of conventional radiotherapy of squamous-cell carcinoma of head and neck: DAHANCA 6 and 7 randomised controlled trial. *Lancet.* 2003;362:933–940.
9. Bonner JA, Harari PM, Giralt J, et al. Radiotherapy plus cetuximab for squamous-cell carcinoma of the head and neck. *N Engl J Med.* 2006;354:567–578.
10. Krause M, Ostermann G, Petersen C, et al. Decreased repopulation as well as increased reoxygenation contribute to the improvement in local control after targeting of the EGFR by C225 during fractionated irradiation. *Radiother Oncol.* 2005;76:162–167.
11. Shields AF, Mankoff DA, Link JM, et al. Carbon-11-thymidine and FDG to measure therapy response. *J Nucl Med.* 1998;39:1757–1762.
12. Shields AF, Grierson JR, Dohmen BM, et al. Imaging proliferation in vivo with [F-18]FLT and positron emission tomography. *Nat Med.* 1998;4:1334–1336.
13. Rasey JS, Grierson JR, Wiens LW, Kolb PD, Schwartz JL. Validation of FLT uptake as a measure of thymidine kinase-1 activity in A549 carcinoma cells. *J Nucl Med.* 2002;43:1210–1217.
14. Sherley JL, Kelly TJ. Regulation of human thymidine kinase during the cell cycle. *J Biol Chem.* 1988;263:8350–8358.
15. Machulla HJ. Simplified labeling approach for synthesizing 3′-deoxy-3′-^{18}F-fluorothymidine. *J Radioanal Nucl Chem.* 2000;243:843–846.
16. Troost EG, Vogel WV, Merkx MA, et al. ^{18}F-FLT PET does not discriminate between reactive and metastatic lymph nodes in primary head and neck cancer patients. *J Nucl Med.* 2007;48:726–735.
17. Vogel WV, Wensing BM, van Dalen JA, Krabbe PF, van den Hoogen FJ, Oyen WJ. Optimised PET reconstruction of the head and neck area: improved diagnostic accuracy. *Eur J Nucl Med Mol Imaging.* 2005;32:1276–1282.
18. Vogel WV, van Dalen JA, Oyen WJ. Adequate evaluation of image registration in hybrid PET/CT [letter]. *J Nucl Med.* 2006;47:1556.
19. Daisne JF, Sibomana M, Bol A, Doumont T, Lonneux M, Gregoire V. Tri-dimensional automatic segmentation of PET volumes based on measured source-to-background ratios: influence of reconstruction algorithms. *Radiother Oncol.* 2003;69:247–250.
20. Barber PR, Vojnovic B, Atkin G, et al. Applications of cost-effective spectral imaging microscopy in cancer research. *J Phys D Appl Phys.* 2003;36:1729–1738.
21. Cobben DC, van der Laan BF, Maas B, et al. ^{18}F-FLT PET for visualization of laryngeal cancer: comparison with ^{18}F-FDG PET. *J Nucl Med.* 2004;45:226–231.
22. de Langen AJ, Klabbers B, Lubberink M, et al. Reproducibility of quantitative ^{18}F-3′-deoxy-3′-fluorothymidine measurements using positron emission tomography. *Eur J Nucl Med Mol Imaging.* 2009;36:389–395.
23. Menda Y, Boles Ponto LL, Dornfeld KJ, et al. Kinetic analysis of 3′-deoxy-3′-^{18}F-fluorothymidine (^{18}F-FLT) in head and neck cancer patients before and early after initiation of chemoradiation therapy. *J Nucl Med.* 2009;50:1028–1035.
24. Daisne JF, Duprez T, Weynand B, et al. Tumor volume in pharyngolaryngeal squamous cell carcinoma: comparison at CT, MR imaging, and FDG PET and validation with surgical specimen. *Radiology.* 2004;233:93–100.
25. Barthel H, Perumal M, Latigo J, et al. The uptake of 3′-deoxy-3′-[^{18}F]fluorothymidine into L5178Y tumours in vivo is dependent on thymidine kinase 1 protein levels. *Eur J Nucl Med Mol Imaging.* 2005;32:257–263.
26. Bading JR, Shields AF. Imaging of cell proliferation: status and prospects. *J Nucl Med.* 2008;49(suppl 2):64S–80S.
27. Dittmann H, Dohmen BM, Paulsen F, et al. [^{18}F]FLT PET for diagnosis and staging of thoracic tumours. *Eur J Nucl Med Mol Imaging.* 2003;30:1407–1412.
28. Kameyama R, Yamamoto Y, Izuishi K, et al. Detection of gastric cancer using ^{18}F-FLT PET: comparison with ^{18}F-FDG PET. *Eur J Nucl Med Mol Imaging.* 2009;36:382–388.
29. Smyczek-Gargya B, Fersis N, Dittmann H, et al. PET with [^{18}F]fluorothymidine for imaging of primary breast cancer: a pilot study. *Eur J Nucl Med Mol Imaging.* 2004;31:720–724.
30. Wang N, He Q, Skog S, Eriksson S, Tribukait B. Investigation on cell proliferation with a new antibody against thymidine kinase 1. *Anal Cell Pathol.* 2001;23:11–19.
31. He Q, Mao Y, Wu J, et al. Cytosolic thymidine kinase is a specific histopathologic tumour marker for breast carcinomas. *Int J Oncol.* 2004;25:945–953.
32. Mao Y, Wu J, Wang N, et al. A comparative study: immunohistochemical detection of cytosolic thymidine kinase and proliferating cell nuclear antigen in breast cancer. *Cancer Invest.* 2002;20:922–931.
33. Mao Y, Wu J, Skog S, et al. Expression of cell proliferating genes in patients with non-small cell lung cancer by immunohistochemistry and cDNA profiling. *Oncol Rep.* 2005;13:837–846.
34. Wu J, Mao Y, He L, et al. A new cell proliferating marker: cytosolic thymidine kinase as compared to proliferating cell nuclear antigen in patients with colorectal carcinoma. *Anticancer Res.* 2000;20(6C):4815–4820.
35. Molthoff CF, Klabbers BM, Berkhof J, et al. Monitoring response to radiotherapy in human squamous cell cancer bearing nude mice: comparison of 2′-deoxy-2′-[^{18}F]fluoro-D-glucose (FDG) and 3′-[^{18}F]fluoro-3′-deoxythymidine (FLT). *Mol Imaging Biol.* 2007;9:340–347.
36. Brockenbrough JS, Rasey JS, Grierson JR, Wiens LW, Vesselle H. A simple quantitative assay for the activity of thymidine kinase 1 in solid tumors. *Nucl Med Biol.* 2007;34:619–623.
37. Wagner M, Seitz U, Buck A, et al. 3′-[^{18}F]fluoro-3′-deoxythymidine ([^{18}F]-FLT) as positron emission tomography tracer for imaging proliferation in a murine B-Cell lymphoma model and in the human disease. *Cancer Res.* 2003;63:2681–2687.